

Sparse Variational Bayesian Approximations for Nonlinear Inverse Problems: applications in nonlinear elastography

I.M. Franck^a, P.S. Koutsourelakis^a

^a*Fachgebiet für Kontinuumsmechanik, Technische Universität München, Boltzmannstrasse 15, 85747 Garching (b. München), Germany*

Abstract

This paper presents an efficient Bayesian framework for solving nonlinear, high-dimensional model calibration problems. It is based on Variational Bayesian formulation that aims at approximating the exact posterior by means of solving an optimization problem in an appropriately selected family of distributions. The goal is two-fold. Firstly, to find lower-dimensional representations of the unknown parameter vector that capture as much as possible of the associated posterior density, and secondly to enable the computation of the approximate posterior density with as few forward calls as possible. We discuss how these objectives can be achieved by using a fully Bayesian argumentation and employing the marginal likelihood or evidence as the ultimate model validation metric for any proposed dimensionality reduction. We demonstrate the performance of the proposed methodology to problems in nonlinear elastography where the identification of the mechanical properties of biological materials can inform non-invasive, medical diagnosis.

Keywords: Uncertainty Quantification, Variational Bayesian, Inverse Problem, Dimensionality reduction, Elastography, Biomaterial Modeling, Dictionary Learning

1. Introduction

The extensive use of large-scale computational models poses several challenges in model calibration as the accuracy of the predictions provided depends strongly on assigning proper values to the various model parameters. In mechanics of materials, accurate mechanical property identification can guide damage detection and an informed assessment of the system's reliability [1]. Identifying

property-cross correlations can lead to the design of multi-functional materials [2]. Permeability estimation for soil transport processes can assist in detection of contaminants, oil exploration [3].

Deterministic optimization techniques which have been developed to address these problems [4, 5, 6, 7, 8, 9], lead to point estimates for the unknowns without rigorously considering the statistical nature of the problem and without providing quantification of the uncertainty in the inverse solution. Statistical approaches based on the Bayesian paradigm, on the other hand aim at computing a (posterior) probability distribution on the parameters of interest. Bayesian formulations offer several advantages as they provide a unified framework for dealing with the uncertainty introduced by the incomplete and noisy measurements and assessing quantitatively inferential uncertainties. Significant successes have been noted in applications such as geological tomography [10, 11], medical tomography [12], hydrology [13], petroleum engineering [14, 15], as well as a host of other physical, biological, or social systems [16, 17, 18, 19]. Representations of the parametric fields in existing deterministic and Bayesian approaches (artificially) impose a minimum length scale of variability usually determined by the discretization size of the governing PDEs [13]. As a result they give rise to a very large vector of unknowns. Inference in high-dimensional spaces using standard Markov Chain Monte Carlo (MCMC) schemes, which for years have served as the workhorse of Bayesian computation, is generally impractical as it requires an exuberant number of calls to the forward simulator in order to achieve convergence. Advanced schemes such as those employing Sequential Monte Carlo samplers [20, 21] or adaptive MCMC [22] can alleviate some of these difficulties particularly when the posterior is multi-modal but still pose significant challenges in terms of the computational cost [?].

This work is particularly concerned with the identification of the mechanical properties of biological materials, in the context non-invasive medical diagnosis. While in certain cases mechanical properties can also be measured directly by excising multiple tissue samples, non-invasive procedures offer obvious advantages in terms of ease, cost and reducing risk of complications to the patient. Rather than x-ray techniques which capture variations in density, the identification of stiffness or mechanical properties in general, can potentially lead to earlier and more accurate diagnosis [23, 24], provide valuable insights that differentiate between modalities of the same pathology [25] and monitor the progress of treatments. In this paper we do not propose new imaging techniques but rather aim at developing rigorous statistical models and efficient computational tools that can make use of the data/observables (i.e. noisy displacements of

deformed tissue) from existing imaging modalities (such as magnetic resonance [26], ultrasonic) in order to produce certifiable estimates of mechanical properties. The primary imaging modality considered in this project is ultrasound elasticity imaging (elastography [27, 28]). It is based on ultrasound tracking of pre- and post-compression images to obtain a map of position changes and deformations of the specimen due to an external pressure/load. The pioneering work of Ophir and coworkers [29] followed by several clinical studies [30, 31, 32, 33] have demonstrated that the resulting strain images typically improve the diagnostic accuracy over ultrasound alone.

Beyond a mere strain imaging there are two approaches for inferring the constitutive material parameters. In the *direct approach*, the equations of equilibrium are interpreted as equations for the material parameters of interest, where the inferred strains and their derivatives appear as coefficients [34]. While such an approach provides a computationally efficient strategy, it does not use the raw data (i.e. noisy displacements) but transformed versions i.e. strain fields (or even-worse, strain derivatives) which arise by applying sometimes ad hoc filtering and smoothing operators. As a result the informational content of the data is compromised and the quantification of the effect of observation noise is cumbersome. Furthermore, the smoothing employed can smear regions with sharply varying properties and hinder proper identification.

The alternative to direct methods, i.e. *indirect or iterative* procedures admit an inverse problem formulation where the discrepancy between observed and model-predicted displacements is minimized with respect to the material fields of interest [35, 36, 37, 38]. While these approaches utilize directly the raw data, they generally imply an increased computational cost as the forward problem and potentially derivatives have to be solved/computed several times. This effort is amplified when stochastic/statistical formulations are employed as those arising in the Bayesian paradigm. Technological advances have led to the development of hand-carried ultrasound systems in the size of a smartphone [39]. Naturally their accuracy and resolution does not compare with the more expensive traditional ultrasound machines or even more so MRI systems. If however computational tools are available that can distill the informational content from noisy and incomplete data then this would constitute a major advance. Furthermore, significant progress is needed in improving the computational efficiency of these tools if they are to be made applicable on a patient-specific basis.

In this work we advocate a Variational Bayesian (VB) perspective [40, 41]. Such methods have risen into prominence for probabilistic inference tasks in the machine learning community [42, 43, 44] but have recently been employed

also in the context of inverse problems [45, 46]. They provide *approximate* inference results by solving an optimization problem over a family of appropriately selected densities with the objective of minimizing the Kullback-Leibler divergence [47] with the exact posterior. The success of such an approach hinges upon the selection of appropriate densities that have the capacity of providing good approximations while enabling efficient (and preferably) closed-form optimization with regards to their parameters.

Critical to the success of VB or any other inference method is dimensionality reduction i.e. the identification of lower-dimensional features that provide the strongest signature to the unknowns and the corresponding posterior. Discovering a sparse set of features has attracted great interest in many applications as in the representation of natural images [48] and a host of algorithms have been developed not only for finding such representations but also an appropriate dictionary for achieving this goal [49, 50, 51, 52]. While all these tools are pertinent to the present problem they differ in a fundamental way. They are based on several data/observations/instantiations of the vector that we seek to represent. In our problem however we do not have such direct observations i.e. the data available pertains to the output of a model which is nonlinearly and implicitly dependent on the vector of unknowns. Furthermore we are primarily interested in approximating the posterior of the this vector rather than the dimensionality reduction itself. *We demonstrate how this can be done by using a fully Bayesian argumentation and employing the marginal likelihood or evidence as the ultimate model validation metric for any proposed dimensionality reduction.*

The paper is organized as follows: The next section (section 2) presents the essential ingredients of the forward model considered which are common with a wide range of nonlinear, high-dimensional problems encountered in several simulation contexts. We also discuss the VB framework advocated, the dimensionality reduction scheme proposed, the prior densities for all model parameters, an iterative, coordinate-ascent algorithm that enables the identification of all the unknowns as well as an information-theoretic criterion for determining the number of dimensions needed. Section 3 demonstrates the performance and features of the proposed methodology in two problems from solid mechanics that are of relevance to the elastography settings. Various signal-to-noise ratios are considered and the performance of the method, in terms of forward calls, is assessed.

2. Methodology

The motivating application is related to continuum mechanics in the non-linear elasticity regime. We describe below the governing equations in terms of conservation laws and the constitutive equations. The proposed model calibration process can be readily adapted to other forward models. As it will be shown, the only information utilized by the Bayesian inference engine proposed is a) the response quantities at the locations where measurements are available, and b) their derivatives with respect to the unknown model parameters.

2.1. Forward model - Governing equations

The following expressions are formulated in the general case which includes nonlinear material behavior and large deformations. Let \mathbf{X} denote the coordinates of the continuum particles in the undeformed configuration and \mathbf{x} in the deformed. Their relation (in the static case) is provided by the deformation map ϕ such that: $\mathbf{x} = \phi(\mathbf{X})$. The displacement field is defined as $\mathbf{u}(\mathbf{X}) = \mathbf{x} - \mathbf{X} = \phi(\mathbf{X}) - \mathbf{X}$. The gradient of the deformation map is denoted by $\mathbf{F} = \nabla\phi$ and $\mathbf{E} = \frac{1}{2}(\mathbf{F}^T\mathbf{F} - \mathbf{I})$ is then the Lagrangian (finite) strain tensor used as the primary kinematic state variable in our constitutive law [53, 54, 55]. The governing equations consist of the conservation of linear momentum:

$$\nabla \cdot (\mathbf{F}\mathbf{S}) + \rho_0\mathbf{b} = 0 \quad (1)$$

where \mathbf{b} is body force vector (per unit mass), ρ_0 is the initial density and \mathbf{S} is the second Piola-Kirchhoff stress tensor. For a hyperelastic material, it is assumed that the strain energy density function $w(\mathbf{E}; \psi)$ depends only on the Lagrangian strain tensor \mathbf{E} and the constitutive material parameters $\psi(\mathbf{X})$. We note that the latter in general have different values at different points in the continuum and at each point, the conjugate stress variables described by the second Piola-Kirchhoff stress tensor can be found as:

$$\mathbf{S} = \frac{\partial w}{\partial \mathbf{E}} = \mathbf{S}(\mathbf{E}; \psi) \quad (2)$$

The aforementioned governing equations should of course be complemented with appropriate boundary conditions and any other information about the problem e.g. incompressibility. In fact incompressibility is frequently encountered in bio-materials and corresponds to the condition $\det(\mathbf{F}) = 1$ at all points in the problem domain.

The governing equations presented thus far cannot be solved analytically for the vast majority of problems and one must resort to numerical techniques that discretize these equations and the associated fields. The most prominent such approach is the Finite Element Method (FEM) which is employed in this study as well. In the first step the *weak* form of the PDEs needs to be derived. Subsequently the problem domain is discretized into finite elements and shape functions are used for interpolating the unknown fields. As this is a very mature subject, from a theoretical and computational point of view, we do not provide further details here but refer the interested reader to one of many books available [56, 57, 58]. Most often all unknowns are expressed in terms of the discretized displacement field denoted here by a vector $\mathbf{U} \in \mathbb{R}^n$. An approximate solution can be found by solving an n -dimensional system of nonlinear algebraic equations which in residual form can be written as:

$$\mathbf{r}(\mathbf{U}; \mathbf{\Psi}) = \mathbf{0} \quad (3)$$

We denote here by $\mathbf{r} : \mathbb{R}^n \times \mathbb{R}^{d_\Psi} \rightarrow \mathbb{R}^n$ the residuals and by $\mathbf{\Psi} \in \mathbb{R}^{d_\Psi}$ the *discretized* vector of constitutive material parameters $\psi(\mathbf{X})$. Such discretizations can be done in many different ways. For example if the same mesh and shape functions as for the discretization of the displacements are adopted, then each entry of the vector $\mathbf{\Psi}$ corresponds to the value of the material parameter of interest at each nodal point. Frequently it is assumed that the value of the constitutive parameters are constant within each finite element in which case d_Ψ coincides with the number of elements in the FE mesh. While the representation of $\mathbf{\Psi}$ is discussed in detail in the sequence, we point out that the discretization of $\psi(\mathbf{X})$ does not need to be associated with the discretization used for the governing equations. Usually in practice the two are related, but if one aims at inferring as many details about the variability of $\psi(\mathbf{X})$ that the discretized equations *Equation(3)* can provide, a finer discretization might be employed for $\psi(\mathbf{X})$. We note however that if the material properties exhibit significant variability within each finite element i.e. if $d_\Psi \gg n$, special care has to be taken in formulating the finite element solution and potential multiscale schemes and sparsity algorithms might need to be employed [59, 60, 61, 62].

We note here:

- Frequently the size n of the system of the equations that need to be solved is large. This is necessitated by accuracy requirements in capturing the underlying physics and mathematics. It can impose a significant computational burden as in general repeated solutions of this system, under different

values of Ψ , are needed. If for a example a Newton-Raphson method is employed then repeated solutions of the linearized Equation (3) will need to be performed:

$$\begin{cases} 0 = \mathbf{r}(\mathbf{U}^{(t)}) + \mathbf{J}(\mathbf{U}^{(t)})\delta\mathbf{U}^{(t)} \\ \mathbf{U}^{(t+1)} = \mathbf{U}^{(t)} + \delta\mathbf{U}^{(t)} \end{cases} \quad (4)$$

where t is the iteration number and $\mathbf{J} = \frac{\partial \mathbf{r}}{\partial \mathbf{U}}$ is the Jacobian matrix. Hence for large n as in applications of interest, the number of such forward solutions is usually what dictates the overall computational cost and this is what we report in subsequent numerical experiments. Depending on the particular solution method employed, converged solutions $\mathbf{U}(\Psi)$ at a certain stage of the inversion procedure can be used as initial guesses for subsequent solutions under different Ψ reducing as a result the overall cost. In this work we do not make use of such techniques.

- The data available generally concerns a subset or more generally a lower-dimensional function of \mathbf{U} . In this work, the experimental measurements/ observations are (noisy) displacements at specific locations in the problem domain. We denote these displacements by $\mathbf{y} \in \mathbb{R}^{d_y}$ and they can be formally expressed as $\mathbf{y} = \mathbf{Q}\mathbf{U}$ where \mathbf{Q} is a Boolean matrix which picks out the entries of interest from \mathbf{U} . Naturally, since \mathbf{U} depends on Ψ , \mathbf{y} is also a function of Ψ i.e. $\mathbf{y}(\Psi)$. We emphasize that this function is generally *highly nonlinear* and most often than not, many-to-one. The unavailability of the inverse as well as the high nonlinearity constitute two of the basic difficulties of the associated inverse problem.
- In addition to the solution vector $\mathbf{U}(\Psi)$, the proposed inference scheme will make use of the derivatives $\frac{\partial \mathbf{y}(\Psi)}{\partial \Psi}$. The computation of derivatives of the response with respect to model parameters is a well-studied subject in the context of PDE-constrained optimization [63, 64, 65] and we make use of it in this work. For any scalar function $f(\mathbf{U})$, one can employ the adjoint form of Equation (3) according to which:

$$\frac{df}{d\Psi_k} = -\nu_j \frac{\partial r_i}{\partial \Psi_k} \quad (5)$$

where $\boldsymbol{\nu} \in \mathbb{R}^n$ is defined such as:

$$\nu_j \frac{\partial r_j}{\partial U_i} = \frac{\partial f}{\partial U_i} \quad \text{or} \quad \mathbf{J}^T \boldsymbol{\nu} = \frac{\partial f}{\partial \mathbf{U}} \quad (6)$$

We note that $\frac{\partial r_j}{\partial U_i}$ is the Jacobian of the residuals in Equation (3) evaluated at the solution $\mathbf{U}(\boldsymbol{\Psi})$. We point out that if a direct solver for the solution of the linear system in Equation(4) is employed, then the additional cost of evaluating $\frac{\partial f}{\partial \boldsymbol{\Psi}}$ is minimal as the Jacobian would not need to be re-factorized for solving Equation (6) ¹. Especially when the dimension d_y of \mathbf{y} is much smaller than that of \mathbf{U} , repeated use of Equation (5) and Equation (6) with f being each of the $y_i, i = 1, \dots, d_y$ can readily yield the desired matrix $\frac{\partial \mathbf{y}}{\partial \boldsymbol{\Psi}}$.

2.2. Bayesian Model

The following discussion is formulated in general terms and can be applied for the calibration of any model with parameters represented by the vector $\boldsymbol{\Psi} \in \mathbb{R}^{d_\Psi}$ when output $\mathbf{y}(\boldsymbol{\Psi}) \in \mathbb{R}^{d_y}$ is available. We also presuppose the availability of the derivatives $\frac{\partial \mathbf{y}}{\partial \boldsymbol{\Psi}}$. For problems of practical interest, it is assumed that the dimension d_Ψ of the unknowns is very large which poses a significant hindrance in the solution of the associated inverse problem as well as in finding proper regularization (in deterministic settings, [66]) or in specifying appropriate priors (in probabilistic settings [67]). The primary focus of the Bayesian model developed is two-fold:

- find lower-dimensional representations of the unknown parameter vector $\boldsymbol{\Psi}$ that capture as much as possible of the associated posterior density
- enable the computation of the posterior density with as few forward calls (i.e. evaluations of $\mathbf{y}(\boldsymbol{\Psi}), \frac{\partial \mathbf{y}}{\partial \boldsymbol{\Psi}}$) as possible.

We denote $\hat{\mathbf{y}} \in \mathbb{R}^{d_y}$ the vector of observations/measurements. In the context of elastography the observations are displacements (in the static case) and/or velocities (in the dynamics). The extraction of this data from images (ultrasound or MRI) is a challenging topic that requires sophisticated image registration techniques [68, 69, 70]. Naturally, these compromise the informational content of

¹The cost of evaluating $\frac{\partial r_i}{\partial \Psi_k}$ is negligible compared to other terms as it scales linearly with the number of elements/nodes

the raw data (i.e. the images). In this study we ignore the error introduced by the image registration process and assume that the displacement data are contaminated with noise. We postulate the presence of i.i.d Gaussian noise denoted here by the random vector $\mathbf{z} \in \mathbb{R}^{d_y}$ such that:

$$\hat{\mathbf{y}} = \mathbf{y}(\Psi) + \mathbf{z}, \quad \mathbf{z} \approx \mathcal{N}(\mathbf{0}, \tau^{-1} \mathbf{I}_{d_y}) \quad (7)$$

We assume that each entry of \mathbf{z} has zero mean and an unknown variance τ^{-1} which will also be inferred from the data. We note that other models can also be employed as for example impulsive noise to account for outliers due to instrument calibration or experimental conditions [71, 72]. Generally the difference between observed and model-predicted outputs can be attributed not only to observation errors (noise) but also to model discrepancies [73, 74?]. In this work we presuppose that the magnitude of this error is much smaller than that of the noise.

The likelihood function of the observed data $\hat{\mathbf{y}}$ i.e. its conditional probability density given the model parameters Ψ (and implicitly the model \mathcal{M} itself as described by the aforementioned governing Equations (3)) and τ is:

$$p(\hat{\mathbf{y}}|\Psi, \tau) = \left(\frac{\tau}{2\pi}\right)^{d_y/2} e^{-\frac{\tau}{2}|\hat{\mathbf{y}}-\mathbf{y}(\Psi)|^2} \quad (8)$$

In the Bayesian framework advocated one would also need to specify priors on the unknown parameters. We defer a detailed discussion of the priors associated with Ψ for the next section where the dimensionality reduction aspects are discussed. With regards to the noise precision τ we employ a Gamma prior i.e.

$$\tau \sim \text{Gamma}(a_0, b_0) \quad (9)$$

The values of the parameters are taken $a_0 = b_0 = 0$ in the following examples. This corresponds to a limiting case where the density degenerates to an improper, non-informative Jeffreys prior i.e. $p(\tau) \propto \frac{1}{\tau}$ that is scale invariant [75]. Naturally more informative choices can be made if such information is available a priori.

2.2.1. Dimensionality Reduction for Ψ

As mentioned earlier one of the primary goals of the present work to is identify a lower-dimensional subspace in \mathbb{R}^{d_Ψ} where the posterior probability density can be sufficiently-well approximated but could also be found with the least number of forward calls. Dimensionality reduction could be enforced directly by appropriate

prior specification. For example in [76] the Fourier transform coefficients of Ψ corresponding to small-wavelength fluctuations were turned-off by assigning zero prior probability to non-zero values. While such an approach achieves the goal of dimensionality reduction it does not take into account the forward model in doing so. The nonlinear map $\mathbf{y}(\Psi)$ as well as the available data $\hat{\mathbf{y}}$ provide different amounts of information for identifying different features of Ψ . One would expect the likelihood (which measures the degree of fit of model predictions with the data) to exhibit different levels of sensitivity along along different directions in the Ψ -space. Consider for example the Maximum-Likelihood-Estimate (MLE) Ψ_{MLE} (or in general a local maximum) in Equation (8). At one extreme, there would be variations from Ψ_{MLE} along directions where even the slightest change would cause a huge drop in the likelihood, and on the other, there would be other variations from Ψ_{MLE} along which the likelihood would remain constant. It is obvious that along the latter directions the posterior in the vicinity of Ψ_{MLE} would be largely determined by the prior whereas in the former directions, the likelihood term would dominate the posterior.

The goal of this work is to identify such directions. We believe however that this effort should not be driven by linear-algebraic objectives with regards to the Hessian of the map $\mathbf{y}(\Psi)$ around Ψ_{MLE} (which might not be unique anyway) as it was done in [77] but it should rather be dictated by probabilistic arguments and the quality of the approximation to the posterior. *We demonstrate how this can be done by using a fully Bayesian argumentation and employing the marginal likelihood or evidence [41] as the ultimate model validation metric for any proposed dimensionality reduction.*

To that end we postulate the following representation for the high-dimensional vector of unknowns Ψ :

$$\underbrace{\Psi}_{d_{\Psi} \times 1} = \underbrace{\mu}_{d_{\Psi} \times 1} + \underbrace{\mathbf{W}}_{d_{\Psi} \times d_{\Theta}} \underbrace{\Theta}_{d_{\Theta} \times 1}. \quad (10)$$

The motivation behind such a decomposition is quite intuitive as it resembles a PCA model [78]. The vector μ represents the mean value of the representation of Ψ whereas Θ the reduced (and latent) coordinates of Ψ along the linear subspace spanned by the d_{Θ} columns of the matrix \mathbf{W} . The linear decomposition of a high-dimensional vector such as Ψ has received a lot of attention in several different fields. Most commonly Ψ represents a high-dimensional signal (e.g. an image, an audio/video recording) and \mathbf{W} consists of an over- or under-complete basis set [79, 80, 52] which attempts to encode the signal as *sparingly* as possible.

Significant advances in Compressed Sensing [81] or Sparse Bayesian Learning [82] have been achieved in recent years along these lines. A host of deterministic [50] or probabilistic [83] algorithms have been developed for identifying the reduced-coordinates Θ (or their posterior) as well as techniques for learning the most appropriate set of basis \mathbf{W} (dictionary learning) i.e. the one that can lead to the sparsest possible representation. While all these tools are pertinent to the present problem they differ in a fundamental way. They are based on several data/ observations/instantiations of Ψ whereas in our problem we do not have such direct observations i.e. the data available pertains to \mathbf{y} which is nonlinearly and implicitly dependent on Ψ . Furthermore we are primarily interested in approximating the posterior on Ψ rather than the dimensionality reduction itself.

Before we embark in the discussion of how these objectives can be achieved we note that an interesting possibility which is not explored here is to use a reduced but continuous representation of the material parameter field(s) $\psi(\mathbf{X})$ directly instead of its discretized representation. In this case one would express $\psi(\mathbf{X})$ as:

$$\psi(\mathbf{X}) = \mu(\mathbf{X}) + \sum_{i=1}^{d_{\Theta}} \Theta_i w_i(\mathbf{X}) \quad (11)$$

where Θ_i play again the role of reduced coordinates as in Equation (10) and $\mu(\mathbf{X})$, $w_i(\mathbf{X})$ are the continuous counterparts of $\boldsymbol{\mu}$ and \mathbf{W} .

We focus now on the representation of Equation(10) and proceed to discuss the identification of $\boldsymbol{\mu}$, \mathbf{W} and Θ . In a fully Bayesian setting these parameters would be equipped with priors and their joint posterior would be sought. Such an inference problem would in general be formidable particularly with regards to $\boldsymbol{\mu}$ and \mathbf{W} whose dimension is dominated by $d_{\Psi} \gg 1$. To overcome this difficulty we propose computing point estimates for $\boldsymbol{\mu}$ and \mathbf{W} while quantifying the posterior of Θ . In doing so for $\boldsymbol{\mu}$ and \mathbf{W} the natural objective function would be the (marginal) likelihood $p(\hat{\mathbf{y}}|\boldsymbol{\mu}, \mathbf{W})$ or in general the posterior $p(\boldsymbol{\mu}, \mathbf{W}|\hat{\mathbf{y}}) = p(\hat{\mathbf{y}}|\boldsymbol{\mu}, \mathbf{W})p(\boldsymbol{\mu}, \mathbf{W})$ where $p(\boldsymbol{\mu}, \mathbf{W})$ is the (joint) prior on $\boldsymbol{\mu}, \mathbf{W}$. In the former case the point estimates for $\boldsymbol{\mu}, \mathbf{W}$ would be the MLE estimates whereas in latter the Maximum-a-Posterior-Estimates (MAP). The difficulty in both cases stems from the likelihood $p(\hat{\mathbf{y}}|\boldsymbol{\mu}, \mathbf{W})$ which requires an integration over Θ and τ . We note here that the (marginal) likelihood or evidence $p(\hat{\mathbf{y}}|\boldsymbol{\mu}, \mathbf{W})$ is the denominator in Bayes' formula for the posterior on (Θ, τ) :

$$p(\Theta, \tau|\hat{\mathbf{y}}, \boldsymbol{\mu}, \mathbf{W}) = \frac{p(\hat{\mathbf{y}}|\Theta, \tau, \boldsymbol{\mu}, \mathbf{W}) p(\Theta) p(\tau)}{p(\hat{\mathbf{y}}|\boldsymbol{\mu}, \mathbf{W})} \quad (12)$$

where $p(\tau)$ represents the Gamma prior for τ discussed previously and $p(\Theta)$ denotes a general prior on Θ that will be made specific in the sequence. Then from Equation (8) we have that:

$$\begin{aligned}
\log p(\hat{\mathbf{y}}|\boldsymbol{\mu}, \mathbf{W}) &= \log \int p(\hat{\mathbf{y}}, \Theta, \tau|\boldsymbol{\mu}, \mathbf{W}) d\Theta d\tau \\
&= \log \int p(\hat{\mathbf{y}}|\Theta, \tau, \boldsymbol{\mu}, \mathbf{W}) p(\Theta) p(\tau) d\Theta d\tau \\
&= \log \int \left(\frac{\tau}{2\pi}\right)^{M/2} e^{-\frac{\tau}{2}|\hat{\mathbf{y}}-\mathbf{y}(\Psi)|^2} p(\Theta) p(\tau) d\Theta d\tau \\
&= \log \int \left(\frac{\tau}{2\pi}\right)^{M/2} e^{-\frac{\tau}{2}|\hat{\mathbf{y}}-\mathbf{y}(\boldsymbol{\mu}+\mathbf{W}\Theta)|^2} p(\Theta) p(\tau) d\Theta d\tau
\end{aligned} \tag{13}$$

The latter equation arises due to Equation (10). We note that such an integration is analytically impossible primarily due to the nonlinear and implicit nature of $\mathbf{y}(\boldsymbol{\mu} + \mathbf{W}\Theta)$ and secondarily due to the coupling of Θ and τ . To alleviate these difficulties we employ the following approximations:

- We linearize the map $\mathbf{y}(\boldsymbol{\mu} + \mathbf{W}\Theta)$ at $\boldsymbol{\mu}$. Hence:

$$\mathbf{y}(\boldsymbol{\mu} + \mathbf{W}\Theta) \approx \mathbf{y}(\boldsymbol{\mu}) + \mathbf{G}\mathbf{W}\Theta \tag{14}$$

where $\mathbf{G} = \frac{\partial \mathbf{y}}{\partial \Psi}|_{\Psi=\boldsymbol{\mu}}$ is the gradient of the map at $\boldsymbol{\mu}$.

As a result the term $|\hat{\mathbf{y}} - \mathbf{y}(\boldsymbol{\mu} + \mathbf{W}\Theta)|^2$ in the exponent of the likelihood becomes quadratic with respect to Θ i.e:

$$\begin{aligned}
|\hat{\mathbf{y}} - \mathbf{y}(\boldsymbol{\mu} + \mathbf{W}\Theta)|^2 &\approx |\hat{\mathbf{y}} - \mathbf{y}(\boldsymbol{\mu}) + \mathbf{G}\mathbf{W}\Theta|^2 \\
&= |\hat{\mathbf{y}} - \mathbf{y}(\boldsymbol{\mu})|^2 - 2(\hat{\mathbf{y}} - \mathbf{y}(\boldsymbol{\mu}))^T \mathbf{G}\mathbf{W}\Theta \\
&\quad + \mathbf{W}^T \mathbf{G}^T \mathbf{G} \mathbf{W} : \Theta \Theta^T
\end{aligned} \tag{15}$$

We note here that a quadratic expression with respect to Θ could also be obtained by considering the 2^{nd} order Taylor series of $|\hat{\mathbf{y}} - \mathbf{y}(\boldsymbol{\mu} + \mathbf{W}\Theta)|^2$ around $\boldsymbol{\mu}$ directly. In particular if we denote by $\mathbf{g} = \frac{\partial |\hat{\mathbf{y}} - \mathbf{y}(\Psi)|^2}{\partial \Psi}|_{\Psi=\boldsymbol{\mu}}$ and $\mathbf{H} = \frac{\partial^2 |\hat{\mathbf{y}} - \mathbf{y}(\Psi)|^2}{\partial \Psi \partial \Psi^T}|_{\Psi=\boldsymbol{\mu}}$, then:

$$\begin{aligned}
|\hat{\mathbf{y}} - \mathbf{y}(\boldsymbol{\mu} + \mathbf{W}\Theta)|^2 &\approx |\hat{\mathbf{y}} - \mathbf{y}(\boldsymbol{\mu})|^2 + \mathbf{g}^T \mathbf{W}\Theta \\
&\quad + \frac{1}{2} \mathbf{W}^T \mathbf{H} \mathbf{W} : \Theta \Theta^T
\end{aligned} \tag{16}$$

The computation of 2^{nd} order derivatives \mathbf{H} can also be addressed within the adjoint framework. We refer the interested reader to [64, 84] as we do not pursue this possibility further in this work. The ensuing expressions are based on Equation (15) but can be readily adjusted to include the terms

in Equation (16) instead ².

- We employ a Variational Bayesian approximation [41] to the integral in Equation (13). We provide further details in the next section. We note that similar approximations have been employed in previous works [46, 71, 85] in order to expedite Bayesian inference. The novel element of this work pertains to the dimensionality reduction that can be achieved.

2.2.2. Variational Bayesian approximation

Consider an arbitrary joint density $q(\Theta, \tau)$ on the latent variables Θ, τ . Then by employing Jensen's inequality one can construct a lower bound to the log-likelihood in Equation (13) as follows:

$$\begin{aligned}
\log p(\hat{\mathbf{y}}|\boldsymbol{\mu}, \mathbf{W}) &= \log \int p(\hat{\mathbf{y}}|\Theta, \tau, \boldsymbol{\mu}, \mathbf{W}) p(\Theta) p(\tau) d\Theta d\tau \\
&= \log \int \frac{p(\hat{\mathbf{y}}|\Theta, \tau, \boldsymbol{\mu}, \mathbf{W}) p(\Theta) p(\tau)}{q(\Theta, \tau)} q(\Theta, \tau) d\Theta d\tau \\
&\geq \int q(\Theta, \tau) \log \frac{p(\hat{\mathbf{y}}|\Theta, \tau, \boldsymbol{\mu}, \mathbf{W}) p(\Theta) p(\tau)}{q(\Theta, \tau)} d\Theta d\tau \quad (17) \\
&= E_q \left[\log \frac{p(\hat{\mathbf{y}}|\Theta, \tau, \boldsymbol{\mu}, \mathbf{W}) p(\Theta) p(\tau)}{q(\Theta, \tau)} \right] \\
&= \mathcal{F}(q(\Theta, \tau), \boldsymbol{\mu}, \mathbf{W})
\end{aligned}$$

It can be readily established that the lower bound $\mathcal{F}(q(\Theta, \tau), \boldsymbol{\mu}, \mathbf{W})$ can be also expressed as [41]:

$$\begin{aligned}
\mathcal{F}(q(\Theta, \tau), \boldsymbol{\mu}, \mathbf{W}) &= E_q \left[\log \frac{p(\hat{\mathbf{y}}|\Theta, \tau, \boldsymbol{\mu}, \mathbf{W}) p(\Theta) p(\tau)}{q(\Theta, \tau)} \right] \\
&= \log p(\hat{\mathbf{y}}|\boldsymbol{\mu}, \mathbf{W}) - KL(q(\Theta, \tau) || p(\Theta, \tau|\hat{\mathbf{y}}, \boldsymbol{\mu}, \mathbf{W})) \quad (18)
\end{aligned}$$

where the latter term represents the Kullback-Leibler (KL) divergence (ref Cover Thomas) between $q(\Theta, \tau)$ and the actual posterior $p(\Theta, \tau|\hat{\mathbf{y}}, \boldsymbol{\mu}, \mathbf{W})$. By definition the KL-divergence is non-negative and it becomes 0 when $q(\Theta, \tau) \equiv p(\Theta, \tau|\hat{\mathbf{y}}, \boldsymbol{\mu}, \mathbf{W})$. Hence constructing a good approximation to the actual posterior (in the KL-divergence sense) is equivalent to maximizing the lower bound $\mathcal{F}(q(\Theta, \tau), \boldsymbol{\mu}, \mathbf{W})$ to the log-likelihood.

In addition this implies that probabilistic inference can be expressed in terms of a parametric optimization. One can adopt a functional form for $q(\Theta, \tau)$ depending on an appropriate set of parameters and identify their optimal value

²The only additional requirement is that \mathbf{H} is semi-positive definite or that a semi-positive approximation $\tilde{\mathbf{H}} \approx \mathbf{H}$ is used

by minimizing the KL-divergence with the posterior or equivalently maximizing \mathcal{F} . In the following we adopt a *mean-field* approximation where the one looks for factorized densities of the form:

$$q(\Theta, \tau) = q(\Theta)q(\tau) \quad (19)$$

Variational mean-field approximations have their origin in statistical physics [86]. One can readily show the optimal factor densities $q^{opt}(\Theta)$ and $q^{opt}(\tau)$ have the form [41]:

$$\begin{aligned} q^{opt}(\Theta) &\propto p(\Theta) e^{E_{q(\tau)}[\log p(\hat{\mathbf{y}}|\Theta, \tau, \mu, \mathbf{W}) - p(\tau)]} \\ q^{opt}(\tau) &\propto p(\tau) e^{E_{q(\Theta)}[\log p(\hat{\mathbf{y}}|\Theta, \tau, \mu, \mathbf{W}) - p(\Theta)]} \end{aligned} \quad (20)$$

We make these expressions more specific in the next sections where we discuss the prior for $p(\Theta)$ as well. We finally note that by making use of the linearization of the map $\mathbf{y}(\Psi)$ and the Variational Bayesian approximation, one can obtain a tractable approximation for the log-likelihood in Equation (8) (and ultimately of the log-posterior $\log p(\mu, \mathbf{W}|\hat{\mathbf{y}})$) while at the same time approximate the posterior of the latent parameters Θ and τ . This will enable us to ultimately identify all model parameters and through this process the optimal subspace for approximating the posterior on Ψ . This will be explained in detail when the final algorithm is presented in section 2.2.4.

We close this section by pointing out that an alternative inference approach for achieving the same objective is the *Laplace approximation* which is based on a semi-analytic Gaussian approximation of the actual posterior $p(\Theta|\hat{\mathbf{y}}, \mu, \mathbf{W})$ in Equation (13). The mean of the Gaussian is set equal to the MAP estimate of Θ_{MAP} and its covariance equal to the inverse of the (approximate) Hessian of the $\log p(\Theta|\hat{\mathbf{y}}, \mu, \mathbf{W})$ at Θ_{MAP} [87, 88, 41, 89]. Even in cases where the posterior is unimodal, the Laplace approximation might yield a poor representation of the nearby probability mass as it is constructed using information only at a single point, Θ_{MAP} [40]. In contrast, the Variational Bayesian method advocated constructs approximations that account for the whole distribution (as it affects the KL-divergence minimization objective) even when a Gaussian density $q(\Theta)$ in Equation (19) is employed.

2.2.3. Prior Specification for Θ , μ and \mathbf{W}

We discuss first the prior specification on \mathbf{W} . Its d_Θ columns \mathbf{w}_i , $i = 1, \dots, d_\Theta$ span the subspace over which an approximation of Ψ is sought. We note that Ψ depends on the product $\mathbf{W}\Theta$ which would remain invariant by appropriate rescaling of each pair of $\mathbf{w}'_i = \alpha_i \mathbf{w}_i$ and $\Theta'_i = \frac{1}{\alpha_i} \Theta_i$ for any α_i . Hence, to resolve

identifiability issues we require that \mathbf{W} is *orthogonal* i.e. $\mathbf{W}^T \mathbf{W} = \mathbf{I}_R$ where \mathbf{I}_{d_Θ} is the d_Θ -dimensional identity matrix. This is equivalent to employing a uniform prior on \mathbf{W} on the Stiefel manifold $V_{d_\Theta}(\mathbb{R}^{d_\Psi})$ [90].

The latent, reduced coordinates $\Theta \in \mathbb{R}^{d_\Theta}$ capture the variation of Ψ around its mean μ along the directions of \mathbf{W} as implied by Equation (10). It is therefore reasonable to assume that, a priori, these should have zero mean and should be uncorrelated [78]. For that purpose we adopt a multivariate Gaussian prior (denoted by $p(\Theta)$ in the Equations of the previous section) with a diagonal covariance denoted by $\Lambda_0 = \text{diag}(\lambda_{0,i}), i = 1, \dots, d_\Theta$. We select prior variances $\lambda_{0,r}^{-1}$ such that $\lambda_{0,1}^{-1} > \lambda_{0,2}^{-1} > \dots > \lambda_{0,d_\Theta}^{-1}$. This induces a natural (stochastic) ordering to the reduced coordinates Θ since Ψ is invariant to permutations of the entries of the Θ and the columns of \mathbf{W} (Equation (10)). As a result of this ordering, Θ_1 is associated with the direction along which the largest variance in Ψ is attained, Θ_2 with the direction with the second largest variance and so on. We discuss the particular values given to prior hyperparameters $\lambda_{0,i}$ in the sequel (Section 2.3) where the possibility of an adaptive decomposition is also presented. This enables the sequential addition of reduced coordinates until a sufficiently good approximation to the posterior is attained.

The final aspect of the prior model pertains to μ . We use a hierarchical prior that induces the requisite smoothness given that Ψ represents the spatial variability of the material parameters. In particular the prior model employed penalizes the jumps in the values of Ψ_k and Ψ_l which correspond to neighboring sites/locations k, l . The definition of a neighborhood can be adjusted depending on the problem, but in this work we assume that sites/locations belong to the neighborhood if they correspond to adjacent pixels/voxels. Suppose d_L is the total number of jumps or neighboring pairs. Then for $j = 1, \dots, d_L$ if k_j and l_j denote the corresponding neighboring pair:

$$p(\mu_{k_j} - \mu_{l_j} | \phi) = \sqrt{\frac{\phi_j}{2\pi}} e^{-\frac{\phi_{k_l}}{2} (\mu_{k_j} - \mu_{l_j})^2} \quad (21)$$

The strength of the penalty is proportional to the hyperparameter ϕ_j , i.e. smaller values of ϕ_j induce a weaker penalty and vice versa. Let \mathbf{L} the $d_L \times d_\Psi$ denote the Boolean matrix that can be used to produce the vector of all d_L jumps (as the one above) between all neighboring sites from the vector Ψ as $\mathbf{L}\Psi$, and $\Phi = \text{diag}(\phi_j)$ the *diagonal matrix* containing all the hyperparameters ϕ_j associated with each of these jumps. We can represent the combined prior on μ

as:

$$p(\boldsymbol{\mu}|\Phi) \propto |\Phi|^{1/2} e^{-\frac{1}{2}\boldsymbol{\mu}^T \mathbf{L}^T \Phi \mathbf{L} \boldsymbol{\mu}} \quad (22)$$

A natural choice for the prior of the hyperparameters Φ is a product of Gamma distributions:

$$p(\Phi) = \prod_{j=1}^{d_L} \text{Gamma}(a_\phi, b_\phi) \quad (23)$$

As in [91] the independence is motivated by the absence of correlation (a priori) with regards to the locations. In this work we use $a_\phi = b_\phi = 0$ which corresponds to a limiting case of a Jeffreys prior that is scale invariant. We note that in contrast to previous works where such priors have been employed for the vector of unknowns Ψ and MAP estimates have been obtained [92], we employ this here for $\boldsymbol{\mu}$ which is only part of the overall decomposition in Equation (10). We discuss in the following section the update equations for $\boldsymbol{\mu}$ and the associated hyper-parameters Φ as well as for the remaining model variables.

2.2.4. Update equations for $q(\Theta)$, $q(\tau)$, $\boldsymbol{\mu}$, \mathbf{W}

This section discusses the optimization with respect to $q(\Theta)$ and $q(\tau)$ for the latent variables as well as the model parameters $\boldsymbol{\mu}$, \mathbf{W} . In the absence of a prior for $\boldsymbol{\mu}$, \mathbf{W} the objective function is the lower bound \mathcal{F} to the log-likelihood in Equation (17). Maximizing \mathcal{F} with regards to $q(\Theta)$ and $q(\tau)$ is equivalent to minimizing their KL-divergence from the actual posterior on Θ and τ as discussed in Equation (18). Maximizing \mathcal{F} with regards to $\boldsymbol{\mu}$, \mathbf{W} leads to approximate MLEs for these parameters. To perform the optimization we propose a coordinate ascent algorithm where we alternate between optimizing \mathcal{F} with regards to one of these variables while keeping the rest fixed as illustrated in Figure 1. We note that in the presence of the priors $p(\boldsymbol{\mu}) = \int p(\boldsymbol{\mu}|\Phi)p(\Phi) d\Phi$ and $p(\mathbf{W})$, the optimization should be carried with the objective $\mathcal{F} + \log p(\boldsymbol{\mu}) + \log p(\mathbf{W})$. This is a lower bound on true log-posterior $\log p(\boldsymbol{\mu}, \mathbf{W}|\hat{\mathbf{y}}) = \log p(\hat{\mathbf{y}}|\boldsymbol{\mu}, \mathbf{W}) + \log p(\boldsymbol{\mu}) + \log p(\mathbf{W})$.

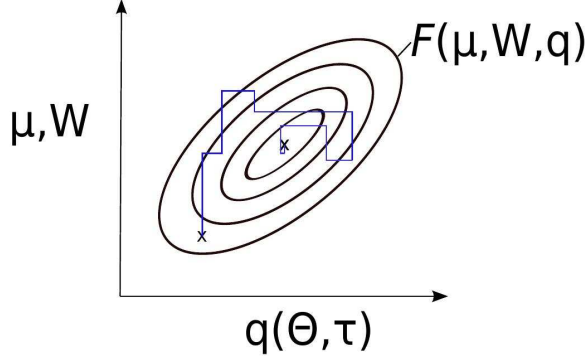


Figure 1: Coordinate ascent: Alternating between optimizations with regards to μ , \mathbf{W} and $q(\Theta, \tau)$.

We postulate first that the reduced coordinates should a posteriori have zero mean as the capture variability around μ . For that purpose we confine our search for $q(\Theta)$ to distributions with zero mean. Given the aforementioned prior $p(\Theta)$ and the linearization discussed in the previous section, we can readily deduce from Equation (20) that the optimal approximate posteriors $q^{opt}(\Theta)$ and $q^{opt}(\tau)$ under the mean-field Variational Bayesian scheme adopted will be:

$$q^{opt}(\Theta) \equiv \mathcal{N}(\mathbf{0}, \mathbf{\Lambda}^{-1}), \quad q^{opt}(\tau) \equiv \text{Gamma}(a, b) \quad (24)$$

The associated parameters are given by the following *iterative* Equations:

$$\begin{aligned} a &= a_0 + N/2 \\ b &= b_0 + \frac{1}{2}|\hat{\mathbf{y}} - \mathbf{y}(\mu)|^2 + \frac{1}{2}\text{tr}(\mathbf{W}^T \mathbf{G}^T \mathbf{G} \mathbf{W} \mathbf{\Lambda}^{-1}) \end{aligned} \quad (25)$$

$$\mathbf{\Lambda} = \mathbf{\Lambda}_0 + \langle \tau \rangle \mathbf{W}^T \mathbf{G}^T \mathbf{G} \mathbf{W} \quad (26)$$

where $\langle \tau \rangle = E_{q^{opt}(\tau)}[\tau] = \frac{a}{b}$.

As a result of the aforementioned Equations and Equation (10), one can establish that the *posterior* of Ψ is approximated by a Gaussian with mean and covariance given by:

$$\begin{aligned} E[\Psi] &= E[\mu + \mathbf{W}\Theta] = \mu + \mathbf{W}\Theta \\ \text{Cov}[\Psi] &= \mathbf{W}\mathbf{\Lambda}^{-1}\mathbf{W}^T \end{aligned} \quad (27)$$

We note that if we diagonalize $\mathbf{\Lambda}^{-1}$ i.e. $\mathbf{\Lambda}^{-1} = \mathbf{V}\mathbf{D}\mathbf{V}^T$ where \mathbf{D} is diagonal

and \mathbf{V} is orthogonal with columns equal to the eigenvectors of $\mathbf{\Lambda}^{-1}$, then:

$$\begin{aligned} Cov[\mathbf{\Psi}] &= \mathbf{WVDV}^T\mathbf{W}^T \\ &= \tilde{\mathbf{W}}\mathbf{D}\tilde{\mathbf{W}}^T \end{aligned} \quad (28)$$

where $\tilde{\mathbf{W}}$ is also orthogonal (i.e. $\tilde{\mathbf{W}}^T\tilde{\mathbf{W}} = \mathbf{I}_{d_\Theta}$) and contains the R principal directions of the posterior covariance of $\mathbf{\Psi}$. Hence it suffices to consider approximate posteriors $q(\Theta)$ with covariance $\mathbf{\Lambda}^{-1}$ that is *diagonal* i.e. $\mathbf{\Lambda} = diag(\lambda_i)$, $i = 1, \dots, d_\Theta$. In this case the update equations for λ_i in Equation (26) reduce to:

$$\lambda_i = \lambda_{0,i} + \langle \tau \rangle \mathbf{w}_i^T \mathbf{G}^T \mathbf{G} \mathbf{w}_i \quad (29)$$

We note that despite the uncorrelated prior assumption on Θ , the posterior on $\mathbf{\Psi}$ exhibits correlation and captures the principal directions along which the variance is largest. Furthermore, implicit to the aforementioned derivations is the assumption of a unimodal posterior on Θ and subsequently on $\mathbf{\Psi}$. This assumption can be relaxed by employing a mixture of Gaussians (e.g. Oxford thesis) that will enable the approximation of highly non-Gaussian and potentially multi-modal posteriors. Such approximations could also be combined with the employment of different basis sets \mathbf{W} for each of the mixture component which would provide a wide range of possibilities. We defer further discussions along these lines to future works. In the current elastography applications, the unimodal assumption seems to be a reasonable one due to the generally large of amounts of data/observations obtained from various imaging modalities.

Given the aforementioned discussion one can obtain an expression for the variational lower bound \mathcal{F} to the log-likelihood in Equation (18). For economy of notation we use $\langle . \rangle$ to imply expectations with respect to $q^{opt}(\Theta)$ and/or $q^{opt}(\tau)$ as implied by the arguments:

$$\begin{aligned} \mathcal{F}(q(\Theta)q(\tau), \boldsymbol{\mu}, \mathbf{W}) &= E_q \left[\log \frac{p(\hat{\mathbf{y}}|\Theta, \tau, \boldsymbol{\mu}, \mathbf{W}) p(\Theta) p(\tau)}{q(\Theta, \tau)} \right] \\ &= -\frac{d_y}{2} \log 2\pi + \frac{d_y}{2} \langle \tau \rangle - \frac{\langle \tau \rangle}{2} \langle |\hat{\mathbf{y}} - \mathbf{y}(\boldsymbol{\mu}) - \mathbf{G} \mathbf{W} \Theta|^2 \rangle \\ &\quad + \frac{1}{2} \log |\mathbf{\Lambda}_0| - \frac{1}{2} \mathbf{\Lambda}_0 : \langle \Theta \Theta^T \rangle \\ &\quad + (a_0 - 1) \langle \log \tau \rangle - b_0 \langle \tau \rangle - \log Z(a_0, b_0) \\ &\quad - \frac{1}{2} \log |\mathbf{\Lambda}| + \frac{R}{2} \\ &\quad - (a - 1) \langle \log \tau \rangle + b \langle \tau \rangle + \log Z(a, b) \end{aligned} \quad (30)$$

where $Z(\gamma, \delta) = \frac{\Gamma(\gamma)}{\delta^\gamma}$ is the normalization constant of a *Gamma* distribution with parameters x, y . The aforementioned equation can be further simplified by making use of the following expectations: $\langle \Theta \rangle = \mathbf{0}$, $\langle \Theta \Theta^T \rangle = \Lambda^{-1}$:

$$\begin{aligned}
\mathcal{F}(q^{opt}(\Theta)q^{opt}(\tau), \boldsymbol{\mu}, \mathbf{W}) &= -\frac{N}{2} \log 2\pi + \frac{N}{2} \langle \tau \rangle - \frac{\langle \tau \rangle}{2} |\hat{\mathbf{y}} - \mathbf{y}(\boldsymbol{\mu})|^2 \\
&\quad - \frac{\langle \tau \rangle}{2} \mathbf{W}^T \mathbf{G}^T \mathbf{G} \mathbf{W} : \Lambda^{-1} \\
&\quad + \frac{1}{2} \log |\Lambda_0| - \frac{1}{2} \Lambda_0 : \Lambda^{-1} \\
&\quad + (a_0 - 1) \langle \log \tau \rangle - b_0 \langle \tau \rangle - \log Z(a_0, b_0) \\
&\quad - \frac{1}{2} \log |\Lambda| + \frac{R}{2} \\
&\quad - (a - 1) \langle \log \tau \rangle + b \langle \tau \rangle + \log Z(a, b)
\end{aligned} \tag{31}$$

In order to update \mathbf{W} , it suffices to consider only the terms of \mathcal{F} that depend on it which we denote by $\mathcal{F}_W(\mathbf{W})$ i.e.:

$$\mathcal{F}_W(\mathbf{W}) = -\frac{\langle \tau \rangle}{2} \mathbf{W}^T \mathbf{G}^T \mathbf{G} \mathbf{W} : \Lambda^{-1} \tag{32}$$

As discussed earlier this should be augmented with $\log p(\mathbf{W})$ which in this case enforces the orthogonality constraint on \mathbf{W} . To that end we employ the constrained optimization algorithm proposed by [93] which requires much fewer iterations resulting in improved computational speed and less computational cost. [93] uses the Cayley transform to preserve the constraint during the optimization. It makes use only first order derivatives:

$$\frac{\partial \mathcal{F}_W}{\partial \mathbf{W}} = -\langle \tau \rangle \mathbf{G}^T \mathbf{G} \mathbf{W} \Lambda^{-1} \tag{33}$$

and a skew-symmetric matrix \mathbf{B} as

$$\mathbf{B} = \frac{\partial \mathcal{F}_W}{\partial \mathbf{W}} \mathbf{W}^T - \mathbf{W} \frac{\partial \mathcal{F}_W}{\partial \mathbf{W}}^T. \tag{34}$$

The update equations are based on a Crank-Nicholson-like scheme and give rise to:

$$\mathbf{W}_{new} = (\mathbf{I} + \frac{\alpha_W}{2} \mathbf{B})^{-1} (\mathbf{I} + \frac{\alpha_W}{2} \mathbf{B}) \mathbf{W}_{old} \tag{35}$$

where α_W is the step size. In order to derive a good step size we use the Barzilai-Borwein scheme [94] which is a non-monotone line search algorithm.

$$\alpha_W = \frac{|tr(\Delta \mathbf{W} \Delta \frac{\partial \mathcal{F}_W}{\partial \mathbf{W}})|}{tr(\Delta \frac{\partial \mathcal{F}_W}{\partial \mathbf{W}}^T \Delta \frac{\partial \mathcal{F}_W}{\partial \mathbf{W}})} \tag{36}$$

where Δ represents the difference between the current parameter values as compared to the previous step. As discussed in detail in [93] the inversion of the $d_\Psi \times d_\Psi$ matrix $(\mathbf{I} + \frac{\alpha\mathbf{W}}{2}\mathbf{B})$ in Equation (35) can be efficiently performed by inverting a matrix of dimension $2d_\Theta$ which is much smaller than d_Ψ . We note that the updates of \mathbf{W} require no forward calls for the computation of $\mathbf{y}(\boldsymbol{\mu})$ or its derivatives \mathbf{G} .

The final component involves the optimization of $\boldsymbol{\mu}$. As with \mathbf{W} we consider only the terms of \mathcal{F} that depend on it which we denote by $\mathcal{F}_\mu(\boldsymbol{\mu})$ i.e.:

$$\mathcal{F}_\mu(\boldsymbol{\mu}) = -\frac{\leq\tau\geq}{2}|\hat{\mathbf{y}} - \mathbf{y}(\boldsymbol{\mu})|^2 \quad (37)$$

Due to the analytical unavailability of $\log p(\boldsymbol{\mu})$ and its derivatives $\frac{\partial \log p(\boldsymbol{\mu})}{\partial \boldsymbol{\mu}}$ we employ here an Expectation-Maximization scheme [95, 96] which we describe in Appendix Appendix A for completeness. The output of this algorithm is also the posterior on the hyperparameters ϕ_j in Equation (21) which capture the locations of jumps in $\boldsymbol{\mu}$ as well as the probabilities associated with them. The cost of the numerical operations is minimal and scales linearly with the number of neighboring pairs d_L . In the following we simply make use of Equations (A.3) without further explanation.

Formally the determination of the optimal $\boldsymbol{\mu}$ would require the derivatives $\frac{\partial \mathcal{F}_\mu(\boldsymbol{\mu})}{\partial \boldsymbol{\mu}}$ in Equation (37). We note that $\mathbf{G} = \frac{\partial \mathbf{y}}{\partial \boldsymbol{\Psi}}|_{\boldsymbol{\Psi}=\boldsymbol{\mu}}$ depends on $\boldsymbol{\mu}$. Hence finding $\frac{\partial \mathcal{F}_\mu(\boldsymbol{\mu})}{\partial \boldsymbol{\mu}}$ would require the computation of second-order derivatives of $\mathbf{y}(\boldsymbol{\Psi})$ which poses significant computational difficulties in the high-dimensional setting considered. To avoid this and *only* for the purpose of the $\boldsymbol{\mu}$ updates, we linearize Equation (37) around the current guess by ignoring the dependence of \mathbf{G} on $\boldsymbol{\mu}$ or equivalently by assuming that \mathbf{G} remains constant in the vicinity of the current guess. In particular, let $\boldsymbol{\mu}^{(t)}$ denote the value of $\boldsymbol{\mu}$ at iteration t , then in order to find the increment $\Delta\boldsymbol{\mu}^{(t)}$, we define the new objective $F_\mu^{(t)}(\Delta\boldsymbol{\mu}^{(t)})$ as follows:

$$\begin{aligned} F_\mu^{(t)}(\Delta\boldsymbol{\mu}^{(t)}) &= F_\mu(\boldsymbol{\mu}^{(t)} + \Delta\boldsymbol{\mu}^{(t)}) + \log p(\boldsymbol{\mu}^{(t)} + \Delta\boldsymbol{\mu}^{(t)}) \\ &= -\frac{\leq\tau\geq}{2}|\hat{\mathbf{y}} - \mathbf{y}(\boldsymbol{\mu}^{(t)} + \Delta\boldsymbol{\mu}^{(t)})|^2 \\ &\quad -\frac{1}{2}(\boldsymbol{\mu}^{(t)} + \Delta\boldsymbol{\mu}^{(t)})^T \mathbf{L}^T \langle \Phi \rangle \mathbf{L}(\boldsymbol{\mu}^{(t)} + \Delta\boldsymbol{\mu}^{(t)}) \quad (38) \\ &\approx -\frac{\leq\tau\geq}{2}|\hat{\mathbf{y}} - \mathbf{y}(\boldsymbol{\mu}^{(t)}) - \mathbf{G}^{(t)}\Delta\boldsymbol{\mu}^{(t)}|^2 \\ &\quad -\frac{1}{2}(\boldsymbol{\mu}^{(t)} + \Delta\boldsymbol{\mu}^{(t)})^T \mathbf{L}^T \langle \Phi \rangle \mathbf{L}(\boldsymbol{\mu}^{(t)} + \Delta\boldsymbol{\mu}^{(t)}) \end{aligned}$$

We note that only there is no approximation with regards to the $p(\boldsymbol{\mu})$ prior term. By keeping only the terms depending on $\Delta\boldsymbol{\mu}^{(t)}$ in the Equation above we

obtain:

$$\begin{aligned}
F_{\mu}^{(t)}(\Delta\mu^{(t)}) = & -\langle \tau \rangle (\Delta\mu^{(t)})^T (\mathbf{G}^{(t)})^T \mathbf{G}^{(t)} \Delta\mu^{(t)} + \langle \tau \rangle (\hat{\mathbf{y}} - \mathbf{y}(\mu^{(t)}))^T \mathbf{G}^{(t)} \Delta\mu^{(t)} \\
& - (\Delta\mu^{(t)})^T \mathbf{L}^T \langle \Phi \rangle \mathbf{L} \Delta\mu^{(t)} \\
& + (\mu^{(t)})^T \mathbf{L}^T \langle \Phi \rangle \mathbf{L} \Delta\mu^{(t)}
\end{aligned} \tag{39}$$

This is a concave and quadratic with respect to the unknown $\Delta\mu^{(t)}$. The maximum can be found by setting $\frac{\partial F_{\mu}^{(t)}(\Delta\mu^{(t)})}{\partial \Delta\mu^{(t)}} = \mathbf{0}$ which yields:

$$(\langle \tau \rangle (\mathbf{G}^{(t)})^T \mathbf{G}^{(t)} + \mathbf{L}^T \langle \Phi \rangle \mathbf{L}) \Delta\mu^{(t)} = \langle \tau \rangle (\mathbf{G}^{(t)})^T (\hat{\mathbf{y}} - \mathbf{y}(\mu^{(t)})) + \mathbf{L}^T \langle \Phi \rangle \mathbf{L} \mu^{(t)} \tag{40}$$

We finally note that the exact objective $F_{\mu}(\mu) + \log p(\mu)$ is evaluated at $\mu^{(t+1)} = \mu^{(t)} + \Delta\mu^{(t)}$ and $\mu^{(t+1)}$ is accepted only if the value of the exact objective is larger than that at $\mu^{(t)}$.

We summarize below the basic steps of the iterative Variational Bayesian scheme proposed in Algorithm 1.

Algorithm 1 Variational Bayesian Approach Including Dictionary Learning

- 1: Initialize μ , \mathbf{W} , Λ_0 and the hyperparameters $a_0, b_0, a_{\phi}, b_{\phi}$
 - 2: **while** \mathcal{F} (Equation (18)) has not been converged **do**
 - 3: Update μ using Equation (40)
 - 4: Update \mathbf{W} using Equations (32-36)
 - 5: Update $q(\Theta) \equiv \mathcal{N}(\mathbf{0}, \Lambda^{-1})$ using Equation (29) and $q(\tau) \equiv \text{Gamma}(a, b)$ using Equation (25)
 - 6: **end while**
-

With regards to the overall computational cost we note that the updates of μ are the most demanding as they require calls to the forward model to evaluate $\mathbf{y}(\mu^{(t)})$ and the derivatives $\mathbf{G}^{(t)} = \frac{\partial \mathbf{y}}{\partial \Psi} |_{\Psi=\mu^{(t)}}$.

2.3. Adaptive learning - Cardinality of reduced coordinates

The presentation thus far was based on a fixed number d_{Θ} of reduced coordinates Θ . A natural question that arises is how many should one consider. In order to address this issue we propose an adaptive learning scheme according to which the analysis is first performed with a few (even one) reduced coordinates and upon convergence additional reduced coordinates are introduced, either in small batches or even one-by-one. Critical to the implementation of such a scheme is

a metric for the progress achieved by the addition of reduced coordinates and basis vectors which can also be used as a termination criterion.

In this work we advocate the use of an information-theoretic criterion which measures the information gain between the prior beliefs on Θ and the corresponding posterior. To measure such gains we employ again the KL-divergence between the aforementioned distributions [97]. In particular if $p_{d_\Theta}(\Theta)$ (section 2.2.3) and $q_{d_\Theta}(\Theta)$ (Equation (29)) denote the d_Θ -dimensional prior and posterior respectively, we define the quantity $I(d_\Theta)$ as follows:

$$I(d_\Theta) = \frac{KL(p_{d_\Theta}(\Theta)||q_{d_\Theta}(\Theta)) - KL(p_{d_\Theta-1}(\Theta)||q_{d_\Theta-1}(\Theta))}{KL(p_{d_\Theta}(\Theta)||q_{d_\Theta}(\Theta))} \quad (41)$$

which measures the (relative) information gain from $d_\Theta - 1$ to d_Θ reduced coordinates. The KL divergence between two distributions p and q is defined with:

$$KL(p||q) = -E_p(\log q) + E_p(\log p) \quad (42)$$

where $E_p(\cdot)$ is the expectation with regards to p . For $p_{d_\Theta}(\Theta) \equiv \mathcal{N}(\mathbf{0}, \Lambda_0^{-1})$ and $q_{d_\Theta}(\Theta) \equiv \mathcal{N}(\mathbf{0}, \Lambda^{-1})$ where Λ_0, Λ are diagonal as explained previously, it follows that:

$$KL(p_{d_\Theta}(\Theta)||q_{d_\Theta}(\Theta)) = \frac{1}{2} \sum_{i=1}^{d_\Theta} \left(-\log\left(\frac{\lambda_i}{\lambda_{0,i}}\right) + \frac{\lambda_i}{\lambda_{0,i}} - 1 \right) \quad (43)$$

and equation (41) becomes:

$$I(d_\Theta) = \frac{\sum_{i=1}^{d_\Theta} \left(-\log\left(\frac{\lambda_i}{\lambda_{0,i}}\right) + \frac{\lambda_i}{\lambda_{0,i}} - 1 \right) - \sum_{i=1}^{d_\Theta-1} \left(-\log\left(\frac{\lambda_i}{\lambda_{0,i}}\right) + \frac{\lambda_i}{\lambda_{0,i}} - 1 \right)}{\sum_{i=1}^{d_\Theta} \left(-\log\left(\frac{\lambda_i}{\lambda_{0,i}}\right) + \frac{\lambda_i}{\lambda_{0,i}} - 1 \right)}. \quad (44)$$

In the simulations performed in section 3, we demonstrate the evolution of this metric as reduced-coordinates/basis vectors are added one-by-one.

3. Numerical examples

The examples presented are concerned with the probabilistic identification of material parameters from displacement data. We demonstrate the efficacy of the proposed methodology in two, two-dimensional cases where synthetic displacement data are utilized. The data are contaminated with noise as discussed in the sequence. The first example is based on a linear elastic material model. The

second example is based on the Mooney-Rivlin material model which is used to model nonlinear and incompressible response.

In the computations we use $\mathbf{m}_0 = 0$, $a_0 = b_0 = a_\phi = b_\phi = 0$. We employ the adaptive learning scheme discussed in section 2.3 whereby reduced-coordinates/basis vectors are added one-by-one. The precision parameter $\lambda_{0,1}$ in the prior for $q(\Theta_1)$ is set to $\lambda_{0,1} = 10^{-10}$ which corresponds to a vague prior. For subsequent basis $i = 2, 3, \dots$ we assign values to the precision parameters $\lambda_{0,i}$ as follows:

$$\lambda_{0,i} = \lambda_{i-1} - \lambda_{0,i-1}, \quad i = 2, 3, \dots \quad (45)$$

We note that λ_{i-1} corresponds to the *posterior* precision for the *previous* reduced coordinate Θ_{i-1} as found in Equation (29) according to which $\lambda_{0,i} = \tau > \mathbf{w}_{i-1}^T \mathbf{G}^T \mathbf{G} \mathbf{w}_{i-1}$. This essentially implies that, a priori, the next reduced coordinate Θ_i will have the precision of the previous one. Since by construction $\mathbf{w}_i^T \mathbf{G}^T \mathbf{G} \mathbf{w}_i > \mathbf{w}_{i-1}^T \mathbf{G}^T \mathbf{G} \mathbf{w}_{i-1}$, we have that $\lambda_{0,i+1} > \lambda_{0,i}$.

3.1. Example 1: Linear elastic material

In the first example we consider a linear, isotropic elastic material model where the stress-strain relation is given by:

$$\mathbf{S} = \mathbb{C} : \mathbf{E}. \quad (46)$$

where \mathbb{C} is the elasticity tensor [54]. It is given by:

$$\mathbb{C} = \frac{E}{(1 + \nu)} \left(\mathbf{I} + \frac{\nu}{(1 - 2\nu)} \mathbf{1} \otimes \mathbf{1} \right) \quad (47)$$

where E is the elastic modulus. The second material parameter is the Poisson's ratio ν which in this example is assumed known ($\nu = 0$). The vector of unknown parameters Ψ consists of the values of the elastic moduli at each finite element. We assume that the elastic modulus can take two values $E_{inclusion}$ and E_{matrix} such that $\frac{E_{inclusion}}{E_{matrix}} = 5$. The ratio is representative of ductal carcinoma in situ in glandular tissue in the breast under a strain of 15% [98]. The spatial distribution of the material is shown in Figure ?? (REFERENCE CONFIGURATION). The problem is $\Omega = (0, L) \times (0, L)$ with $L = 10$ units. We employ a 10×10 FE mesh. Displacement boundary conditions are employed which resemble those encountered when static pressure is applied on a tissue with the ultrasound transducer invoking a 1% strain as depicted in Figure ?? CHANGE y to x)2. In particular the boundary displacements at the bottom ($x_2 = 0$) are set to zero and at the

top ($x_2 = 10$) the vertical displacements are set to -0.1 . The displacements along the sides ($x_1 = 0$ and $x_1 = 10$) are also assumed zero. The parameter values are at the top row of elements are assumed known and equal to the exact values (E_{matrix}) otherwise any solutions for which $\frac{E_{inclusion}}{E_{matrix}} = 5$ would yield the same likelihood [99]. The displacements generated using the reference configuration were subsequently contaminated with Gaussian noise such that the resulting Signal-to-Noise ratio was $SNR = 10^5$.

The posterior mean can be seen in figure ?? for 90 bases (equal to the total number of unknowns) and in figure ??b) shows the diagonal cut through ??a) and three times of the standard derivation of the material properties. In figure ??c) one sees the information gain over the number of bases where also the number of forward calls is visible. For deriving the posterior with 9 bases 50 forward calls were needed. In the first update 23 forward calls and in the following always 3 forward calls per new basis. However, μ did not changed when adding a new basis so the three forward calls were done to check if any further optimization is possible/needed.

In the next figure, figure ??, one sees the outcome for the same example but for 9 bases. In figure ?? one can see how the posterior develops by adding addition bases and that is converges fast. Compare also figure ?? to see the number of μ -calls, which includes the expensive forward calls, during the development of the posterior. In the right column it is visible that the \mathbf{W} -update, with the Barzilai-Borwein step size selection, is non-monotone but robust.

3.2. Incompressible Mooney-Rivlin material

Nonlinear, hyperelastic models have been successfully used in the past to describe the behavior of several biomaterials [100, 101, 102]. In this example we employ the Mooney-Rivlin model [103, 104] that is characterized by the following strain energy density function w (Equation (2)):

$$w = c_1(\hat{I}_1 - 3) + c_2(\hat{I}_2 - 3) + \frac{1}{2}\kappa(\log J)^2. \quad (48)$$

κ is the bulk modulus, $J = \det(\mathbf{F})$ and $\hat{I}_1 = \frac{I_1}{J^{2/3}}$, $\hat{I}_2 = \frac{I_2}{J^{4/3}}$ where I_1, I_2 are the first and second invariants of the of the left Cauchy-Green deformation tensor $\mathbf{b} = \mathbf{F}\mathbf{F}^T$. The last term is related to volumetric deformations whereas the first two terms to distortional. We consider here an *incompressible* material i.e. $J = 1$ in which case the bulk modulus κ plays the role of a penalty parameter that enforces this constraint. We employ the three-field Hu-Washizu principle

in order to enforce incompressibility and suppress volumetric locking [105, 106]. The three-field formulation requires a separate integration rule for the dilatational stiffness contribution. The bulk modulus is chosen as a function of c_1 with $\kappa = \kappa_0 c_1$. We use $\kappa_0 = 1000$ [105, 107]. The higher κ_0 the stronger is the incompressibility constraint.

In this example we assume $c_2 = 0$ which reduces the model to an uncoupled version of the incompressible neo-Hookean model [54]. The remaining parameter c_1 is assumed to vary in the problem domain which can be seen in Figure ???. In this example we have two inclusions, an elliptic and a circular inclusion, with different material properties. In the larger, elliptic inclusion $c_1 = 4000$ (red), in the smaller, circular inclusion $c_1 = 3000$ (orange) and in the remaining material $c_1 = 1000$ (blue). The problem domain is $\Omega = (0, L) \times (0, L)$ with $L = 50$. It is discretized with 200×200 finite elements of equal size and the governing equations are solved under plane strain conditions. The following boundary conditions are employed: both displacements are set to zero at the bottom ($y = 0$) and on the sides ($x = 0$ and $x = 50$) and a vertical distributed load $f = -100$ in the vertical direction (pointing downwards) is applied along the top i.e. $y = 50$. The displacements found are contaminated with Gaussian noise. The following SNRs were considered: ?. The forward model for the Bayesian identification employed a regular 50×50 mesh and only the corresponding (noisy) displacements at the nodes were used as data (\hat{y}). We note that due to the different meshes employed the data will also contain model errors. We further assumed that c_1 was constant within each of the elements which resulted in $d_\Theta = 2500$ unknowns.

In all following figures the quantities are depicted in the log- scale. In figure xx one can see the posterior distribution with xx bases and in figure xxx the three most important bases. In the next figures the outcome for a noise level of XXX is visible.

The posterior mean μ_{reg} is in excellent agreement with the exact solution and the standard deviation raises as the noise level increases.

4. Conclusions

VB exhibits low computational complexity... and the approximation of the posterior is calibrated by minimizing the Kullback-Leibler divergence. We have shown that...

We introduced in this paper a new algorithm to find a sparse representation with an underdetermined dictionary. With a new dictionary learning algorithm

the few basis vectors in the selected dictionary are improved. Embedded in a variational Bayesian approach no sampling methods are necessary.
 mention possibilities for multi-resolution and mixture

Appendix A. Expectation-Maximization for the μ prior

Due to the analytical unavailability of $\log p(\mu)$ and its derivatives $\frac{\partial \log p(\mu)}{\partial \mu}$ we employ here an Expectation-Maximization scheme which we describe in here for completeness [95, 96]. Proceeding as in Equation (17) i.e. by making use of Jensen's inequality and an arbitrary distribution $q(\Phi)$ we can bound $\log p(\mu)$ as follows:

$$\begin{aligned}
 \log p(\mu) &= \log \int p(\mu|\Phi)p(\Phi) d\Phi \\
 &= \log \int \frac{p(\mu|\Phi)p(\Phi)}{q(\Phi)} q(\Phi) d\Phi \\
 &\geq \int q(\Phi) \log \frac{p(\mu|\Phi)p(\Phi)}{q(\Phi)} d\Phi \\
 &= E_{q(\Phi)}[\log p(\mu|\Phi)] + E_{q(\Phi)}[\log \frac{p(\Phi)}{q(\Phi)}]
 \end{aligned} \tag{A.1}$$

The inequality above becomes an equality only when $q(\Phi) \equiv p(\Phi|bs\mu)$ i.e. it is the actual posterior on Φ given μ . The latter can be readily established from Equations (21) and (23) based on which $p(\Phi|bs\mu) = \prod_{j=1}^{d_L} \text{Gamma}(a_{\phi_j}, b_{\phi_j})$ where:

$$a_{\phi_j} = a_{\phi} + \frac{1}{2}, \quad b_{\phi_j} = b_{\phi} + \frac{1}{2}(\mu_{k_j} - \mu_{k_j})^2 \tag{A.2}$$

This suggests a two-step procedure for computing $\log p(\mu)$ and $\frac{\partial \log p(\mu)}{\partial \mu}$ for each μ :

(E-step) Find $p(\Phi|bs\mu) = \prod_{j=1}^{d_L} \text{Gamma}(a_{\phi_j}, b_{\phi_j})$ from Equation (A.2)

(M-step) Find $\log p(\mu)$ and $\frac{\partial \log p(\mu)}{\partial \mu}$ from Equation (A.1) for $q(\Phi) \equiv p(\Phi|\mu)$ as follows:

$$\begin{aligned}
 \log p(\mu) &= E_{q(\Phi)}[\log p(\mu|\Phi)] = -\frac{1}{2}\mu^T \mathbf{L}^T \langle \Phi \rangle \mathbf{L} \mu \\
 \frac{\partial \log p(\mu)}{\partial \mu} &= \frac{\partial}{\partial \mu} E_{q(\Phi)}[\log p(\mu|\Phi)] \\
 &= E_{q(\Phi)}[\frac{\partial}{\partial \mu} \log p(\mu|\Phi)] \\
 &= -\mathbf{L}^T \langle \Phi \rangle \mathbf{L} \mu
 \end{aligned} \tag{A.3}$$

where $\langle \Phi \rangle = E_{q(\Phi)}[\text{diag}(\phi_j)] = \text{diag}(\frac{a_{\phi_j}}{b_{\phi_j}})$

References

- [1] G. Johannesson, R. Glaser, C. Lee, J. J. Nitao, W. Hanley, Multi-resolution markov-chain-monte-carlo approach for system identification with an application to finite-element models, Tech. rep., Lawrence Livermore National Lab., Livermore, CA (2005).
- [2] S. Torquato, Random Heterogeneous Materials, Springer-Verlag, 2002.
- [3] J. Wang, N. Zabarar, A markov random field model of contamination source identification in porous media flow, INTERNATIONAL JOURNAL OF HEAT AND MASS TRANSFER 49 (5-6) (2006) 939 – 950.
- [4] A. Tikhonov, V. Arsenin, Solution of ill-posed problems, John Wiley & Sons, 1977.
- [5] C. Groetsch, Inverse Problems in the Mathematical Sciences, Vieweg, 1993.
- [6] H. Engl, M. Hanke, A. Neubauer, Regularization of Inverse Problems., Kluwer Academic Publishing, 1996.
- [7] C. Vogel, Computational Methods for Inverse Problems, Frontiers in Applied Mathematics Series, SIAM, 2002.
- [8] D. Calvetti, L. Reichel, Tikhonov regularization of large linear problems, BIT Numerical Mathematics 43 (2) (2003) 263 – 283.
- [9] J. Kaipio, E. Somersalo, Computational and Statistical Methods for Inverse Problems, Springer-Verlag, New York, 2005.
- [10] R. Glaser, G. Johannesson, S. Sengupta, B. Kosovic, S. Carle, Stochastic engine final report: Applying markov chain monte carlo methods with importance sampling to large-scale data-driven simulation, Tech. rep., Lawrence Livermore National Lab., Livermore, CA (2004).
- [11] K. Andersen, S. Brooks, M. B. Hansen, Bayesian inversion of geoelectrical resistivity data, Tech. rep., Dept. Math. Sci., Aalborg University (2001).
- [12] I. Weir, Fully bayesian reconstructions from single-photon emission computed tomography data, JOURNAL OF THE AMERICAN STATISTICAL ASSOCIATION 92 (437) (1997) 49 – 60.

- [13] H. Lee, D. Higdon, Z. Bi, M. Ferreira, M. West, Markov random field models for high-dimensional parameters in simulations of fluid flow in porous media, *TECHNOMETRICS* 44 (3) (2002) 230 – 241.
- [14] B. Hegstad, H. Omre, Uncertainty in production forecasts based on well observations, seismic data, and production history, *SPE JOURNAL* 6 (4) (2001) 409 – 424.
- [15] P. Craig, M. Goldstein, J. Rougier, A. Seheult, Bayesian forecasting for complex systems using computer simulators, *JOURNAL OF THE AMERICAN STATISTICAL ASSOCIATION* 96 (454) (2001) 717 – 729.
- [16] P. Kitanidis, Parameter uncertainty in estimation of spatial functions - bayesian-analysis, *WATER RESOURCES RESEARCH* 22 (4) (1986) 499 – 507.
- [17] D. Schmidt, J. George, C. Wood, Bayesian inference applied to the electromagnetic inverse problem, *HUMAN BRAIN MAPPING* 7 (3) (1999) 195 – 212.
- [18] J. Wang, N. Zabarar, Hierarchical bayesian models for inverse problems in heat conduction, *INVERSE PROBLEMS* 21 (1) (2005) 183 – 206.
- [19] F. Liu, M. Bayarri, J. Berger, R. Paulo, J. Sacks, A bayesian analysis of the thermal challenge problem, *COMPUTER METHODS IN APPLIED MECHANICS AND ENGINEERING* 197 (29-32) (2008) 2457 – 2466.
- [20] P. D. Moral, A. Doucet, A. Jasra, Sequential monte carlo for bayesian computation (with discussion), In *Bayesian Statistics 8*. Oxford University Press.
- [21] P. Koutsourelakis, A multi-resolution, non-parametric, Bayesian framework for identification of spatially-varying model parameters, *Journal of Computational Physics* 228 (17) (2009) 6184–6211.
- [22] N. Chopin, T. Lelivre, G. Stoltz, Free energy methods for bayesian inference: efficient exploration *Statistics and Computing* 22 (4) (2012) 897–916.
doi:10.1007/s11222-011-9257-9.
URL <http://link.springer.com/article/10.1007/s11222-011-9257-9>

- [23] A. A. Oberai, N. H. Gokhale, S. Goenezen, P. E. Barbone, T. J. Hall, A. M. Sommer, J. Jiang, Linear and nonlinear elasticity imaging of soft tissue in vivo: demonstration of feasibility, *PHYSICS IN MEDICINE AND BIOLOGY* 54 (5) (2009) 1191–1207. doi:10.1088/0031-9155/54/5/006.
- [24] N. Ganne-Carrié, M. Ziol, V. de Ledinghen, C. Douvin, P. Marcellin, L. Castera, D. Dhumeaux, J. Trinchet, M. Beaugrand, Accuracy of liver stiffness measurement for the diagnosis of cirrhosis in patients with chronic liver diseases., *Hepatology* 44 (6) (2006) 1511–1517.
- [25] C. Curtis, et al., The genomic and transcriptomic architecture of 2,000 breast tumours reveals no Nature.
URL doi:10.1038/nature10983
- [26] R. Muthupillai, D. Lomas, P. Rossman, J. Greenleaf, A. Manduca, R. Ehman, Magnetic resonance elastography by direct visualization of propagating acoustic strain waves, *Science* 269 (5232) (1995) 1854–1857.
- [27] A. Sarvazyan, T. Hall (Eds.), *Elasticity Imaging Part I & II*, Vol. 7,8, *Cur. Med. Imag. Rev.*, 2011, 2012.
- [28] M. Doyley, Model-based elastography: a survey of approaches to the inverse elasticity problem, *Physics in Medicine and Biology* 35 (2012) 34–73.
doi:10.1088/0031-9155/57/3/R35.
URL <http://iopscience.iop.org/0031-9155/57/3/R35>
- [29] J. Ophir, I. Cespedes, H. Ponnekanti, Y. Yazdi, X. Li, Elastography - a quantitative method for imaging the elasticity of biological tissues, *ULTRASONIC IMAGING* 13 (2) (1991) 111 – 134.
- [30] B. Garra, E. Cespedes, J. Ophir, S. Spratt, R. Zuurbier, C. Magnant, M. Pennanen, Elastography of breast lesions: Initial clinical results 202 (1) (1997) 79 – 86.
- [31] J. Bamber, P. Barbone, N. Bush, D. Cosgrove, M. Doyely, F. Fuechsel, P. Meaney, N. Miller, T. Shiina, F. Tranquart, Progress in freehand elastography of the breast, *IEICE Trans. Inf. Sys.* E85D (1) (2002) 5 – 14.
- [32] A. Thomas, T. Fischer, H. Frey, R. Ohlinger, S. Grunwald, J. Blohmer, K. Winzer, S. Weber, G. Kristiansen, B. Ebert, S. Kummel, Real-time elastography - an advanced method of ultrasound: first results in 108

patients with breast lesions, *Ultrasound Obst. Gyn.* 28 (3) (2006) 335 – 340.

- [33] K. Parker, M. M. Doyley, D. Rubens, Imaging the elastic properties of tissue: the 20 year perspective, *Phys. Med. Biol.*
- [34] P. E. Barbone, C. E. Rivas, I. Harari, U. Albocher, A. A. Oberai, Y. Zhang, Adjoint-weighted variational formulation for the direct solution of inverse problems of general linear elasticity with full interior data, *Int. J. Num. Meth. Eng.* 81 (13) (2010) 1713–1736. doi:10.1002/nme.2760.
- [35] A. Oberai, N. Gokhale, M. Doyley, J. Bamber, Evaluation of the adjoint equation based algorithm for elasticity imaging, *PHYSICS IN MEDICINE AND BIOLOGY* 49 (13) (2004) 2955–2974. doi:10.1088/0031-9155/49/13/.
- [36] M. Doyley, S. Srinivasan, E. Dimidenko, N. Soni, J. Ophir, Enhancing the performance of model-based elastography by incorporating additional a priori information in the modulus image reconstruction process, *PHYSICS IN MEDICINE AND BIOLOGY* 51 (1) (2006) 95–112. doi:10.1088/0031-9155/51/1/007.
- [37] A. Arnold, S. Reichling, O. Bruhns, J. Mosler, Efficient computation of the elastography inverse problem by combining variational mesh adaption and a clustering technique, *PHYSICS IN MEDICINE AND BIOLOGY* 55 (7) (2010) 2035–2056. doi:10.1088/0031-9155/55/7/016.
- [38] L. G. Olson, R. D. Throne, Numerical simulation of an inverse method for tumour size and location estimation, *Inv. Prob. Sc. Eng.* 18 (6) (2010) 813–834. doi:10.1080/17415977.2010.497965.
- [39] S. Schleder, L.-M. Dendl, A. Ernstberger, M. Nerlich, P. Hoffstetter, E.-M. Jung, P. Heiss, C. Stroszczyński, A. G. Schreyer, Diagnostic value of a hand-carried ultrasound device for free intra-abdominal fluid and organ lacerations, *Emergency Medicine Journal* 30 (3) (2013) e20–e20. doi:10.1136/emmermed-2012-201258. URL <http://emj.bmj.com/cgi/doi/10.1136/emmermed-2012-201258>
- [40] M. Beal, Variational algorithms for approximate Bayesian inference (May) (2003) 1–281. URL <http://www.cse.buffalo.edu/faculty/mbeal/papers/beal03.pdf>

- [41] C. Bishop, Pattern recognition and machine learning, 2006.
URL <http://www.library.wisc.edu/selectedtocs/bg0137.pdf>
- [42] M. I. Jordan, Z. Ghahramani, T. S. Jaakkola, S. Cruz, L. K. Saul, F. Park, An Introduction to Variational Methods for Graphical Models (617) (1999) 1–52.
- [43] H. Attias, A Variational Bayesian Framework for Graphical Models.
- [44] M. Wainwright, M. Jordan, Graphical models, exponential families, and variational inference, in: Foundations and Trends in Machine Learning, Vol. 1 of 1-305, 2008, pp. 1–305.
- [45] M. Chappell, A. Groves, B. Whitcher, M. Woolrich, Variational bayesian inference for a nonlinear forward model, IEEE Transactions on Signal Processing 57 (1) (2009) 223–236. doi:10.1109/TSP.2008.2005752.
- [46] B. Jin, J. Zou, Hierarchical Bayesian inference for ill-posed problems via variational method, Journal of Computational Physics 229 (19) (2010) 7317–7343. doi:10.1016/j.jcp.2010.06.016.
URL <http://linkinghub.elsevier.com/retrieve/pii/S0021999110003311>
- [47] T. Cover, J. Thomas, Elements of Information Theory, John Wiley & Sons, 1991.
- [48] B. Olshausen, Emergence of simple-cell receptive field properties by learning a sparse code for natural images, Nature.
URL <http://people.cs.umass.edu/~eshelham/files/papers/olshausen-field-emergence.pdf>
- [49] M. S. Lewicki, T. J. Sejnowski, Learning overcomplete representations., Neural computation 12 (2) (2000) 337–65.
URL <http://www.ncbi.nlm.nih.gov/pubmed/10636946>
- [50] H. Lee, A. Battle, R. Raina, A. Y. Ng, Efficient sparse coding algorithms, in: B. Schlkopf, J. C. Platt, T. Hoffman (Eds.), Advances in Neural Information Processing Systems 19, Proceedings of the Twentieth Annual Conference on Neural Information Processing Systems, Vancouver, British Columbia, Canada, December 4-7, 2006, MIT Press, 2006, pp. 801–808.
- [51] J. Mairal, F. Bach, J. Ponce, G. Sapiro, Online dictionary learning for sparse coding, Proceedings of the 26th

- Annual International Conference on Machine Learning - ICML '09 (2009)
 1–8doi:10.1145/1553374.1553463.
 URL <http://portal.acm.org/citation.cfm?doid=1553374.1553463>
- [52] N. Dobigeon, J.-Y. Tournet, Bayesian orthogonal component analysis for sparse representation, *IEEE Transactions on Signal Processing* 58 (5) (2010) 2675–2685. doi:10.1109/TSP.2010.2041594.
- [53] Holzapfel, *Nonlinear Solid Mechanics* (2000).
- [54] G. Mase, G. Mase, *Continuum mechanics for engineers*, 2010.
 URL http://books.google.com/books?hl=en&lr=&id=uI1110A8B_UC&oi=fnd&pg=PA1&dq=
- [55] J. Bonet, A. Gil, R. Wood, *Worked Examples in Nonlinear Continuum Mechanics for Finite Elements*, 2012.
 URL <http://books.google.com/books?hl=en&lr=&id=zwo-FicSE3sC&oi=fnd&pg=PR8&dq=>
- [56] O. Zienkiewicz, R. Taylor, J. Zhu, *The finite element method: its basis and fundamentals*. 2005, Butterworth-Heinemann, Oxford.
 URL <http://scholar.google.com/scholar?hl=en&btnG=Search&q=intitle:The+Finite+>
- [57] K. Bathe, *Finite element procedures*, 1996.
 URL <https://gforge.sci.utah.edu/gf/project/cibc/scmsvn/?action=browse&path=%2>
- [58] T. Hughes, *The finite element method: linear static and dynamic finite element analysis*.
 URL <http://scholar.google.com/scholar?hl=en&btnG=Search&q=intitle:The+Finite+>
- [59] T. Hughes, G. Feijoo, L. Mazzei, J. Quincy, The variational multiscale method - a paradigm for computational mechanics, *COMPUTER METHODS IN APPLIED MECHANICS AND ENGINEERING* 166 (1-2) (1998) 3 – 24.
- [60] T. Hou, X. Wu, A multiscale finite element method for elliptic problems in composite materials and porous media, *JOURNAL OF COMPUTATIONAL PHYSICS* 134 (1) (1997) 169 – 189.
- [61] M. Dorobantu, B. Engquist, Wavelet-based numerical homogenization, *SIAM Journal of Numerical Analysis* 35 (2) (1998) 540.

- [62] A. Abdulle, Analysis of a heterogeneous multiscale FEM for problems in elasticity, *MATHEMATICAL MODELS & METHODS IN APPLIED SCIENCES* 16 (4) (2006) 615 – 635.
- [63] M. Giles, N. Pierce, An introduction to the adjoint approach to design, *Flow, turbulence and combustion* (2000) 393–415.
URL <http://link.springer.com/article/10.1023/A:1011430410075>
- [64] M. Hinze, R. Pinnau, M. Ulbrich, S. Ulbrich, *Optimization with PDE constraints*, Springer, New York, 2009.
- [65] D. I. Papadimitriou, K. C. Giannakoglou, Direct, adjoint and mixed approaches for the computation of Hessian in airfoil design problems, *International journal for ...* (September 2007) (2008) 1929–1943.
doi:10.1002/flid.
URL <http://onlinelibrary.wiley.com/doi/10.1002/flid.1584/abstract>
- [66] D. Calvetti, L. Reichel, Tikhonov regularization of large linear problems, *BIT Numerical Mathematics* 43 (2) (2003) 263 – 283.
- [67] J. Bardsley, Gaussian markov random field priors for inverse problems, *Inverse Problems and Imaging* 7 (2) (2013) 397–416.
doi:10.3934/ipi.2013.7.397.
URL <https://aimsciences.org/journals/displayArticlesnew.jsp?paperID=8635>
- [68] M. Richards, Quantitative three dimensional elasticity imaging.
URL <http://dcommon.bu.edu/xmlui/handle/2144/1442>
- [69] J. E. Lindop, 2D and 3D Elasticity Imaging Using Freehand Ultrasound - PhD. (March).
- [70] H. Rivaz, E. Boctor, Real-time regularized ultrasound elastography, *Medical Imaging, IEEE ...*
URL http://ieeexplore.ieee.org/xpls/abs_all.jsp?arnumber=5629442
- [71] B. Jin, A variational Bayesian method to inverse problems with impulsive noise, *Journal of Computational Physics* 231 (2) (2012) 423–435.
doi:10.1016/j.jcp.2011.09.009.
URL <http://linkinghub.elsevier.com/retrieve/pii/S0021999111005298>

- [72] S. Godsill, P. Rayner, Statistical reconstruction and analysis of autoregressive signals in impulsive
 IEEE Transactions on Speech and Audio Processing 6 (4) (1998) 352–372.
 doi:10.1109/89.701365.
 URL <http://ieeexplore.ieee.org/lpdocs/epic03/wrapper.htm?arnumber=701365>
- [73] S. R. Arridge, J. P. Kaipio, V. Kolehmainen, M. Schweiger, E. Somersalo, T. Tarvainen, M. Vauhkonen,
 Approximation errors and model reduction with an application in optical diffusion tomography,
 Inverse Problems 22 (1) (2006) 175–195.
 doi:10.1088/0266-5611/22/1/010.
 URL <http://stacks.iop.org/0266-5611/22/i=1/a=010?key=crossref.0d39f8df6743a89>
- [74] J. Kaipio, E. Somersalo, Statistical inverse problems: Discretization, model reduction and inverse
 Journal of Computational and Applied Mathematics 198 (2) (2007) 493–
 504. doi:10.1016/j.cam.2005.09.027.
 URL <http://linkinghub.elsevier.com/retrieve/pii/S0377042705007296>
- [75] D. Lindley, Bayesian statistics: A review, 1972.
 URL <http://epubs.siam.org/doi/pdf/10.1137/1.9781611970654.fm>
- [76] M. Honarvar, R. S. Sahebjavaher, S. E. Salcudean, R. Rohling, Sparsity
 regularization in dynamic elastography, Physics in Medicine and Biology
 57 (19) (2012) 5909–5927. doi:10.1088/0031-9155/57/19/5909.
- [77] T. Bui-Thanh, C. Burstedde, O. Ghattas, J. Martin, G. Stadler,
 L. Wilcox, Extreme-scale UQ for bayesian inverse problems governed
 by PDEs, in: High Performance Computing, Networking, Storage and
 Analysis (SC), 2012 International Conference for, 2012, pp. 1–11.
 doi:10.1109/SC.2012.56.
- [78] M. Tipping, C. M. Bishop, Probabilistic principal component analysis,
 Journal of the Royal Statistical Society B 61 (1999) 611–622.
- [79] B. a. Olshausen, D. J. Field, Natural image statistics and efficient coding.,
 Network (Bristol, England) 7 (2) (1996) 333–9.
 doi:10.1088/0954-898X/7/2/014.
 URL <http://www.ncbi.nlm.nih.gov/pubmed/16754394>
- [80] R. G. Baraniuk, Compressive Sensing (July) (2007) 118–121.

- [81] E. Candès, J. Romberg, T. Tao, Robust uncertainty principles: Exact signal reconstruction from highly incomplete frequency information, *IEEE Trans. Information Theory* 52 (2006) 489–509.
- [82] D. P. Wipf, B. D. Rao, Sparse bayesian learning for basis selection, *IEEE Transactions on Signal Processing* 52 (8) (2004) 2153–2164.
- [83] M. Seeger, D. Wipf, Variational bayesian inference techniques, *IEEE Signal Processing Magazine* 27 (6) (2010) 81–91. doi:10.1109/MSP.2010.938082.
- [84] T. Bui-Thanh, O. Ghattas, D. Higdon, Adaptive hessian-based nonstationary gaussian process response surface method for probability density estimation, *SIAM Journal on Scientific Computing* 34 (6) (2012) A2837–A2871. doi:10.1137/110851419. URL <http://epubs.siam.org/doi/abs/10.1137/110851419>
- [85] M. Chappell, a.R. Groves, B. Whitcher, M. Woolrich, Variational Bayesian Inference for a Nonlinear Forward Model, *IEEE Transactions on Signal Processing* 57 (1) (2009) 223–236. doi:10.1109/TSP.2008.2005752. URL <http://ieeexplore.ieee.org/lpdocs/epic03/wrapper.htm?arnumber=4625948>
- [86] Parisi, *Statistical field theory*, 1988.
- [87] D. Mackay, Probable networks and plausible predictions a review of practical Bayesian methods for network inference, *Journal of the Royal Society Series B* Vol. 6, 1995. doi:10.1088/0954-898X/6/3/011. URL <http://www.informaworld.com/openurl?genre=article&doi=10.1088/0954-898X/6/3/011>
- [88] D. MacKay, Choice of basis for Laplace approximation, *Machine learning* (1998) 1–10. URL <http://link.springer.com/article/10.1023/A:1007558615313>
- [89] C. Oh, J. Beck, M. Yamada, Bayesian learning using automatic relevance determination prior with application to structural reliability analysis, *Journal of engineering mechanics* 134 (12) (2008) 1013–1020. URL [http://ascelibrary.org/doi/abs/10.1061/\(ASCE\)0733-9399\(2008\)134:12\(1013\)](http://ascelibrary.org/doi/abs/10.1061/(ASCE)0733-9399(2008)134:12(1013))
- [90] R. J. Muirhead, *Aspects of Multivariate Statistical Theory*, Wiley, 1982.

- [91] J. Bardsley, D. Calvetti, E. Somersalo, Hierarchical regularization for edge-preserving reconstruction of PET images, *Inverse Problems*.
URL <http://iopscience.iop.org/0266-5611/26/3/035010>
- [92] J. Kaipio, E. Somersalo, *Computational and Statistical Methods for Inverse Problems*, Applied Mathematical Sciences.
URL <http://scholar.google.com/scholar?hl=en&btnG=Search&q=intitle:Computational>
- [93] Z. Wen, W. Yin, A feasible method for optimization with orthogonality constraints, *Mathematical Programming*.
URL <http://link.springer.com/article/10.1007/s10107-012-0584-1>
- [94] J. Barzilai, J. Borwein, Two-point step size gradient methods, *IMA Journal of Numerical Analysis*
URL <http://imajna.oxfordjournals.org/content/8/1/141.short>
- [95] A. P. Dempster, N. M. Laird, D. B. Rubin, Maximum likelihood from incomplete data via the EM algorithm (with discussion), *Journal of the Royal Statistical Society B* 39 (1) (1977) 1–38.
- [96] R. Neal, G. Hinton, A view of the EM algorithm that justifies incremental, sparse, and other variants, in: M. Jordan (Ed.), *Learning in Graphical Models*, Dordrecht: Kluwer Academic Publishers, 1998, pp. 355–368.
- [97] L. Itti, P. Baldi, Bayesian surprise attracts human attention, *Advances in neural information processing systems*
URL http://machinelearning.wustl.edu/mlpapers/paper_files/NIPS2005_199.pdf
- [98] P. Wellman, R. Howe, Breast tissue stiffness in compression is correlated to histological diagnosis, *Harvard BioRobotics* . . . (1999) 1–15.
URL <https://biorobotics.harvard.edu/pubs/1999/mechprops.pdf>
- [99] N. H. Gokhale, P. E. Barbone, A. A. Oberai, Solution of the nonlinear elasticity imaging inverse problem: the compressible case, *INVERSE PROBLEMS* 24 (4). doi:10.1088/0266-5611/24/4/045010.
- [100] A. Samani, D. Plewes, A method to measure the hyperelastic parameters of ex vivo breast tissue, *Physics in Medicine and Biology* 49 (18) (2004) 4395–4405.
doi:10.1088/0031-9155/49/18/014.
URL <http://stacks.iop.org/0031-9155/49/i=18/a=014?key=crossref.4a8069c8c53067>

- [101] J. J. O'Hagan, A. Samani, Measurement of the hyperelastic properties of 44 pathological ex vivo Physics in medicine and biology 54 (8) (2009) 2557–69.
doi:10.1088/0031-9155/54/8/020.
URL <http://www.ncbi.nlm.nih.gov/pubmed/19349660>
- [102] A. a. Oberai, N. H. Gokhale, S. Goenezen, P. E. Barbone, T. J. Hall, A. M. Sommer, J. Jiang, Linear and nonlinear elasticity imaging of soft tissue in vivo: demonstration of feasibility., Physics in medicine and biology 54 (5) (2009) 1191–207.
doi:10.1088/0031-9155/54/5/006.
URL <http://www.pubmedcentral.nih.gov/articlerender.fcgi?artid=3326410&tool=pm>
- [103] M. Mooney, A Theory of Large Elastic Deformation, Journal of Applied Physics 11 (9) (1940) 582. doi:10.1063/1.1712836.
URL <http://scitation.aip.org/content/aip/journal/jap/11/9/10.1063/1.1712836>
- [104] R. Rivlin, Large elastic deformations of isotropic materials. IV. Further developments of the general theory. ... Transactions of the Royal Society of London. Series B, Biological Sciences 241 (835) (1948) 379–397.
URL <http://rsta.royalsocietypublishing.org/content/241/835/379.short>
- [105] J. Simo, R. Taylor, Quasi-incompressible finite elasticity in principal stretches. Continuum basis and numerical implementation. Computer Methods in Applied Mechanics and Engineering 26 (1988) 231–251.
URL <http://www.sciencedirect.com/science/article/pii/004578259190100K>
- [106] O. Zienkiewicz, R. Taylor, The Finite Element Method: Solid Mechanics, 2000.
URL <http://books.google.com/books?hl=en&lr=&id=MhgBfMWFVHUC&oi=fnd&pg=PR13&dq=The+Finite+Element+Method:+Solid+Mechanics>
- [107] M. Schöberl, Technische Universität München (3600392).